IJMT. Vol. 21, Iss. 1, 2025. (44-53)

International Journal of Maritime Technology

Journal homepage: ijmt.ir

Investigation on hydrodynamic effects of using a supercavitating section in surface piercing hydrofoils

Mohammad Amin Esabat[1], **Ahmadreza Kohansal**[2*]

[1] *M.Sc. Student, Persian Gulf University; m.amin.esabat@gmail.com*
[2] *Assistant Professor, Department of Marine Engineering, Persian Gulf University; kohansal@pgu.ac.ir*

ARTICLE INFO

Article History:
Received: 9 Apr 2025
Last modification: 9 Apr 2025
Accepted: 17 Jun 2025
Available online: 17 Jun 2025

Article type:
Research paper

Keywords:
Super-cavitation
Hydrofoil
Surface piercing
Ventilation

ABSTRACT

The purpose of this paper was to numerically investigate the effects of using supercavitation sections in ventilated semi-submerged hydrofoils. Studying the flow around such hydrofoils is often very complicated due to its multiphase nature and the simultaneous occurrence of cavitation and ventilation phenomena. The desired foil was the Waid section foil which has been examined at different attack angles and for different cavitation numbers. In this numerical simulation, the RANSE finite volume solver along with the VOF method have been used to model the multiphase flow around the semi-submerged hydrofoil. According to the obtained results, the formation of cavitation bubbles and the formation of ventilation around a supercavitating section is different from the conventional sections in semi-immersed foils. This could be due to the specific geometric shape of the supercavitating sections, especially in their front area. The pressure and flow contours around the hydrofoil have been predicted in semi-submerged form, and the ventilating air flow around the hydrofoil has also been investigated. Also, it has shown that the effect of cavitation at high speeds causes the formation of continuous bubbles, which will lead to the reduction of drag coefficients and increase the efficiency of supercavitating hydrofoils. According to the results obtained in this simulation, by increasing the cavitation number, the drag coefficient also increases in proportion to the lift coefficient. This process continues until the foil enter the completely wet phase, which with this phase change, the lift-to-drag coefficient ratio also decreases. Therefore, due to its high efficiency, the Waid section, is recommended for the design of surface piercing hydrofoils.

ISSN: 2645-8136

DOI: http://dx.doi.org/10.61882/ijmt.21.1.44

1. Introduction

Usually, with the increase in the speed of hydrofoil vessels, the formation of cavitation around their hydrofoils is inevitable. Water turns into vapor as a result of increasing temperature, but this phenomenon can also occur with decreasing pressure. In other words, when the fluid flow pressure falls below the saturated vapor pressure, vapor bubbles form. This phenomenon is usually called cavitation. In most cases, cavitation has been a very harmful and undesirable phenomenon in marine industries. However, if small cavitation bubbles expand due to a significant reduction in local pressure, they can form a continuous and extensive bubble that acts as insulation against the fluid, creating what is known as supercavitation. This type of cavitation -supercavitation- can be highly desirable and does not have the damaging effects of regular cavitation.

In recent years, researchers have introduced special foil sections under the title of supercavitating sections, which are different from conventional sections in terms of shape and hydrodynamic behavior. It can be said that, the use of special supercavitating sections can lead to a phase change from water to vapor at a low cavitation number, which will lead to a relative reduction in drag and a noticeable increase in lift.

Since the 1950s, studies in this field have led to the development of specific geometries for these types of hydrofoils, which have improved their performance over time. These studies have not only resulted in a reduction in drag coefficient but have also increased the lift-to-drag ratio by guiding the flow on the surface of the body [1]. Given that the viscosity and density of gases and vapors are significantly lower than that of liquids, this phenomenon leads to a substantial reduction in the drag force acting on an object. Exploiting this advantage of cavitation, it is used as a factor to increase speed and improve efficiency [2].

One of the first applications that can be mentioned for supercavitating sections was the use of these sections in marine propellers. It can be said that Tulin was the first one who researched in this field in a professional way. He has developed and expanded the design of supercavitating propellers. However, his efforts did not lead to the application of supercavitating hydrofoils [3].

The significance of supercavitating sections can be observed in Allison's work [4]. He compared the maximum efficiency of various propulsion systems in maritime industries. He showed that the different propulsion systems have varying efficiencies at different speeds. For speeds below 50 knots, fully submerged propellers have the best performance, and even water jets cannot compete at this speed. At higher speeds, such as 60 knots and above, semi-submerged supercavitating propellers have the best performance.

Sharp from Philadelphia, United States, constructed the first semi-submerged propeller for shallow waters. Over time, these propellers have also been used for hydrofoil vessels, and even high-speed ships have incorporated Sharp's propeller design. Given the advanced features of semi- submerged propellers, they are now used in maritime competitions as well. Also, these propellers are put into service in next-generation ships with speeds ranging from 70 to 80 knots [4]. Studies in this field were also conducted by Karman on hydrofoils with NACA 66- 012 and NACA 4412 sections. In his experiments, he achieved a lift-to-drag ratio of 10 [5].

In addition, Yao-tsu provided a theoretical explanation for this phenomenon in curved and flat surfaces [6]. But it can be said that the turning point in research in this field occurred in Forrester studies. He concluded that as the flow behind hydrofoils becomes more turbulent, the lift-to-drag ratio decreases compared to the laminar flow [7].

The study of the surface piercing objects with the different sections and determining the necessary conditions for the formation of ventilation on them was a subject that was taken into consideration by some researchers [8, 9]. Matveev et al. [10] researched the methods of improving the performance and removing ventilation of surface-piercing hydrofoils numerically. Brizzolara et al. [11] investigated the surface piercing hydrofoils and the effect of cavitation and ventilation on them. Also, the two-phase flow around the surface piercing hydrofoils has been studied by some researchers [12, 13]. Several researchers have conducted research on the topic of supercavitating hydrofoils and have introduced several supercavitating sections [14 – 16]. Also, in addition to designing or optimizing the shape of this type of hydrofoils, some researchers tried to analyze their behavior [17-22]

Brizzolara [23] attempted to increase the lift-to-drag ratio of hydrofoils by modifying an existing super-cavitation section. He introduced a section that was suitable for use in surface piercing hydrofoils. According to Brizzolara, in sections of the SCSB 5-25 family, by adding sequence flow to the rear of the hydrofoil, the flow changes from severe turbulence to relatively laminar flow

Varengo et al. [24] presented a supercavitating cross-section and then analyzed it using the boundary element method. Numerical simulation of surface piercing semi-ogive hydrofoil and their effects of the trailing edge configuration and the angles of attack on the natural ventilation, supercavitation and the hydrodynamic forces was done by Wang et al. [25]. They reported the regional ventilated and gas leakage modes.

In this study, the supercavitating sections have been studied as one of the sections that can be used in ventilated semi-submerged hydrofoils. Also, by examining the Waid section, the hydrodynamic behavior of these hydrofoils was investigated. The

supercavitating section was examined in angles of attack ranging from 1 to 7 degrees with cavitation numbers ranging from 0.05 to 0.9. Ultimately, a lift-to-drag ratio of 35 was achieved under semi-submerged conditions.

2. Mathematical and numerical methods

In this study, a RANS solver has been used for flow modeling and VOF method has been used for free surface simulation. This solver solves mass and momentum continuity equations for incompressible flow analysis (Eq. 1).

$$\begin{cases} \nabla \cdot V = 0 \\ \rho V = -\nabla P + \mu \Delta V + \nabla T_{Re} + S_M \end{cases} \quad (1)$$

where V is the average flow velocity, P is the average pressure field, μ is the dynamic viscosity, T_{Re} is the Reynolds stress tensor, and S_M is the momentum source vector.

To simulate the flow with supercavitation, the finite volume method and the SIMPLE algorithm, along with the multiphase cavitation model, have been used. The multiphase model includes the standard viscous flow equations (Navier-Stokes) and the k- RNG turbulence model. The continuity and momentum equations, along with the transport equation and turbulence model equations, form the system of equations that calculates the fluid density.

It is necessary to use a suitable grid for the simulation of flow around the hydrofoil as well as the simulation of the third phase (water vapor). In other words, the total size and number of mesh layers around the hydrofoil and the growth rate of these layers should be such that it is possible to model the creation of the cavitation bubbles around the hydrofoil. For accurate simulation, we are forced to use an accurate and extensive mesh in the refinement area. This is not only because of the importance of representing the free water surface, which is also effective in the results, but also because in this simulation, we use the VOF technique to represent water vapor as accurately as possible.

Figures 1 to 3 show the mesh of the hydrofoil surface, the computational domain and refinement mesh, respectively.

(a)

(b)

Fig. 1: Hydrofoil mesh, (a) cross-sectional view (b) Three-dimensional view of the Waid foil mesh.

(a)

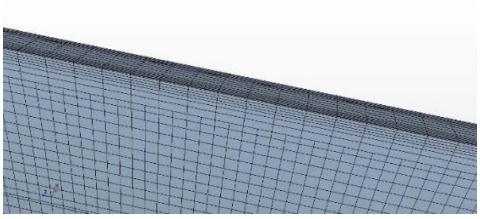

(b)

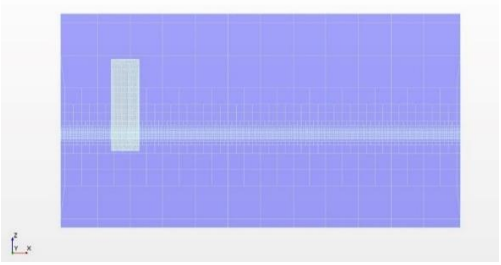

Fig. 2: Three-dimensional view of mesh (a) the hydrofoil's backside (b) tank mesh

The maximum thickness of the prism layer mesh is equal to the thickness of the foil diameter. The minimum distance from the first prism boundary to the surface is considered to be 0.01 meter. It should be noted that in this simulation, the trimmer mesh and the prism and remeshing meshes are used [26, 27]. The mesh on the hull surface also has a maximum and minimum size of 0.0017 meters. However, for better meshing, the foil surface has been divided into smaller sections and each section meshed separately. This way, we also use sections of the body lines for better meshing.

(a)

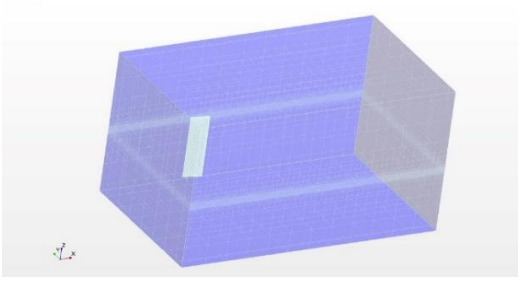

(b)

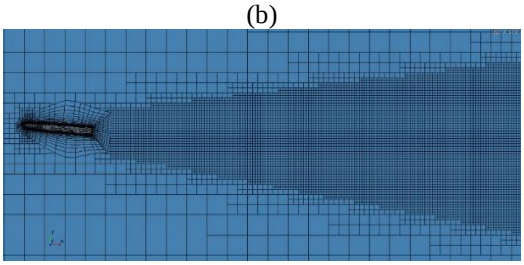

Fig. 3: (a) Three-dimensional view of the tank mesh (b) the top view of the wake mesh

In the refinement mesh, a trimmer mesh with values of 0.003 meters was used for optimal meshing along the X and Z coordinate axes. To improve the refinement mesh, the wake mesh was also used. In this type of mesh, a mesh size of 0.01 meters with a length of 2.1 meters along the X-axis and a mesh angle of 4 degrees as selected for simulating the foil. Figure 3 shows the wake mesh behind the hydrofoil. The results obtained from the numerical solution should be independent of the grid.

One of the cross-sections presented for semi-submerged hydrofoils is the section introduced by Casey Harwood [28], who investigated the effect of angle of attack and Froude number in a semi-submerged form in this foil. A view of this section is shown in Figure 4.

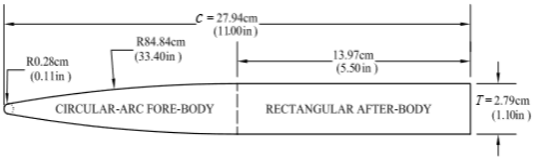

Fig. 4: A view of the Casey Harwood's foil [28]

In the first step, numerical simulation is performed with different number of meshes, which are shown in Table 1. For this purpose, the results of drag and lift coefficients in the simulation of Casey Harwood's foil for 3 angles of attack, 2.5 degrees, 7.5 degrees, and 12.5 degrees are presented with different mesh values (Fig. 5). In the other word, the Casey Harwood's foil was examined in three simulation cases for three angles of attack and at different speeds. The results show that the first and second simulation results change with different mesh values. However, these values in the third, fourth, and fifth simulations remain constant, indicating that the simulation results are independent of the mesh values. Then a mesh value of 1256055 could be sufficient for this simulation.

Figure 6 shows the Y+ contour around the Waid hydrofoil. In this contour, the areas at the tip of the hydrofoil, which are at the water surface and at the end of the hydrofoil, have the highest Y+ values. This value is less than 5 at the hydrofoil surface.

Table 1: Number of meshes in different simulation cases

Case	Case1	Case 2	Case 3	Case 4	Case 5
Mesh Num.	825622	1056606	1256055	1306655	1503655

For a better understanding of the initiation of cavitation, we consider a small spherical nucleus filled with gas within a liquid. Due to surface tension effects, the pressure inside the bubble is higher than outside of it.

(a)

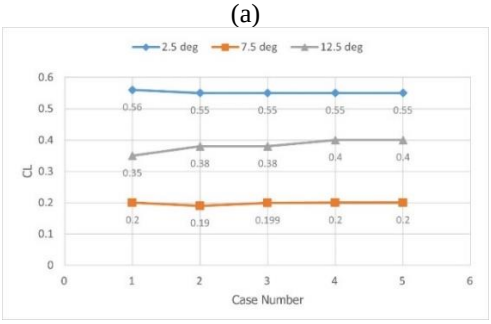

(b)

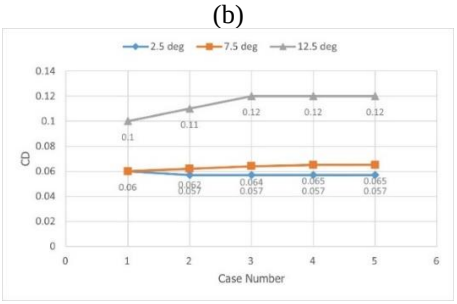

Fig. 5: (a) Lift and (b) drag coefficients at different angles of attack as a function of mesh number of Casey Harwood's foil

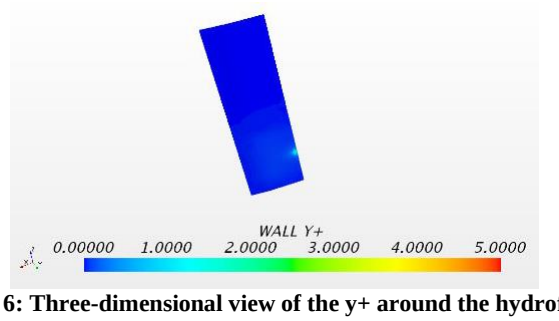

Fig. 6: Three-dimensional view of the y+ around the hydrofoil with the Waid section

The external pressure of the bubble can drop below zero while the internal pressure of the bubble remains positive. If the external pressure decreases to a point where it exceeds the surface tension effect, then the internal pressure of the bubble will decrease, causing rapid vaporization and bubble formation. This leads to bubble instability. If we consider a spherical bubble with a core of radius R, the difference in pressure between the inside and outside of the bubble in a static state can be given by the following equation:

$$\Delta P = P_{in} - P_{out} = \frac{2\sigma}{R0} \quad (2)$$

In the above equation, σ represents surface tension, and P_{out} and P_{in} are the external and internal pressures of the bubble, respectively. Now, if this initial nucleus is introduced into an environment where the internal pressure matches the vapor pressure of the surrounding liquid, it is evident that the liquid making up the core will vaporize and penetrate the nucleus. As a result, the nucleus will grow, and a bubble will form. This can be expressed as:

$$P_v \geq P_{in} = P_{out} + \Delta P \quad (3)$$

Therefore, when P_{out} becomes less than the vapor pressure minus ΔP, the critical pressure for cavitation initiation is reached:

$$P_c \approx P_v - \frac{2\sigma}{R} \quad (4)$$

where R_0 is the largest radius of the core. As observed from these relationships, the stability of the growing bubble depends on its radius and the pressure difference. If this bubble suddenly enters a high-pressure environment, its walls will not withstand the impact, and the bubble will collapse. Additionally, this scenario can occur when the bubble collides with obstacles [29].

3. Results and Discussions

In Figures 7-11, results related to the numerical results of lift and drag coefficients obtained from the simulation of Casey Harwood's foil at four attack angles of 2.5, 7.5, 12.5 and 15 degrees and at two different depths of 0.1397 and 0.2794 meters have been compared with the experimental results. From the comparison of the numerical and experimental results, it is clear that the numerical method has been able to model the problem with relatively good accuracy and the error rate of the numerical method is within an acceptable limit.

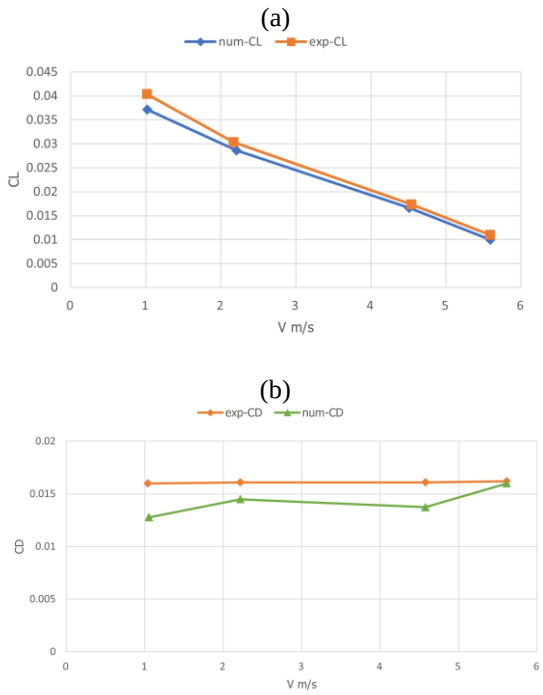

Fig. 7: (a) lift and (b) drag coefficients at an angle of attack of 2.5 degrees and at a depth (an altitude) of 0.1397 m versus speed for Casey Harwood's foil

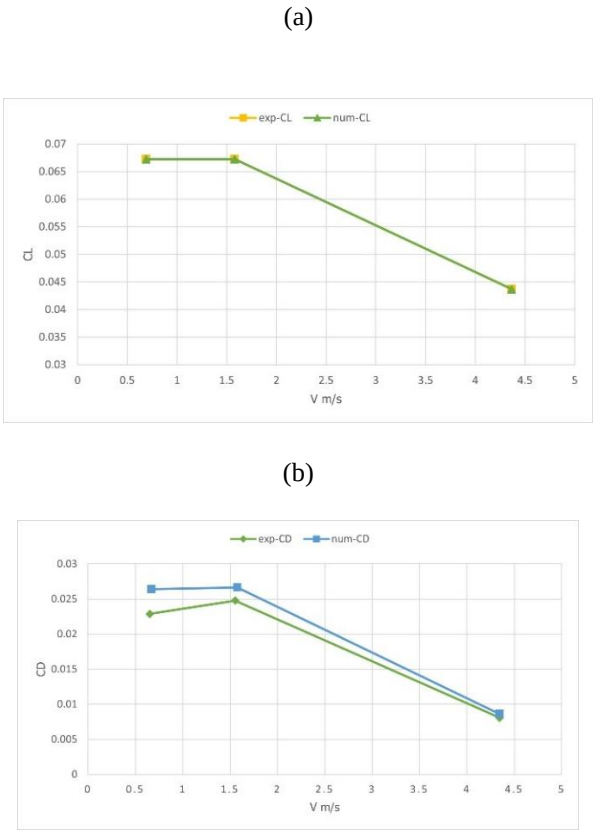

Fig. 8: (a) lift and (b) drag coefficients at an angle of attack of 2.5 degrees at an altitude of 0.2794 m for Casey Harwood's foil

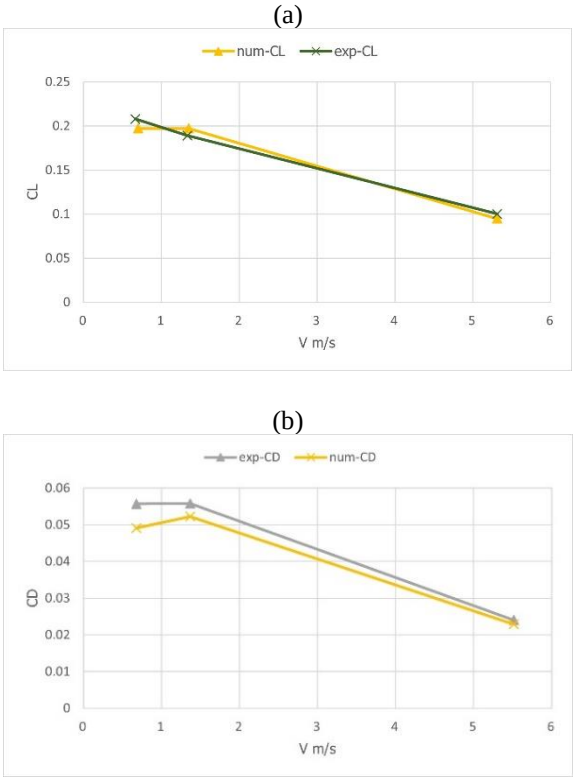

Fig. 9: (a) lift and (b) drag coefficients at an angle of attack of 7.5 degrees at an altitude of 0.27940 m for Casey Harwood's foil

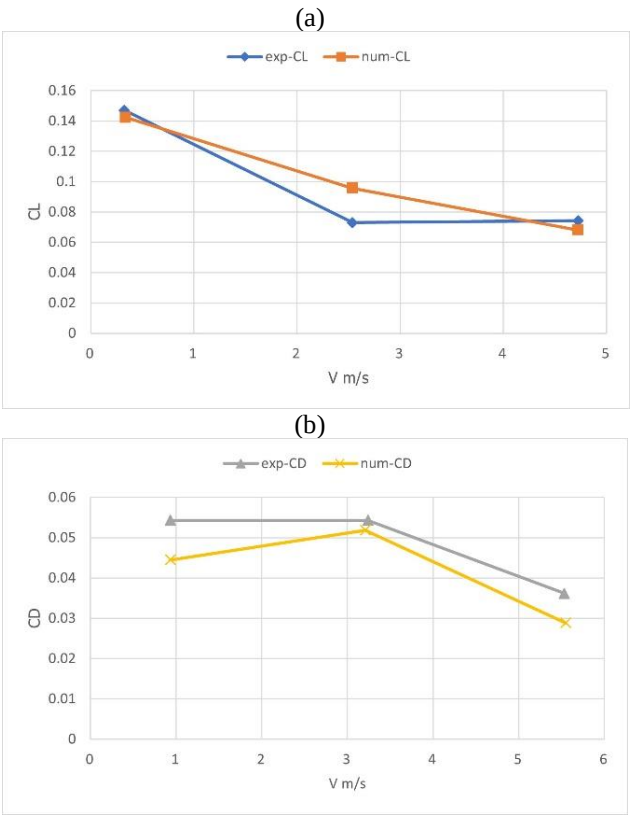

Fig. 10: (a) lift and (b) drag coefficients at an angle of attack of 12.5 degrees at an altitude of 0.2794 m for Casey Harwood's foil

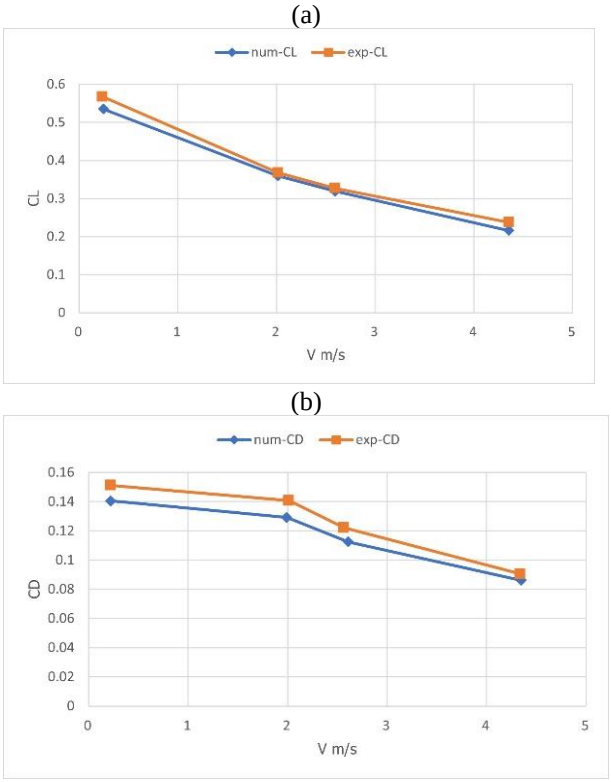

Fig. 11: (a) lift and (b) drag coefficients at an angle of attack of 15 degrees at an altitude of 0.2794 for Casey Harwood's foil

As previously mentioned, the purpose of this research was modeling and numerical simulation of a surface piercing hydrofoil with a Waid section. The Waid hydrofoil was simulated at angles of 1, 3, 5, and 7 degrees and at speeds of 15, 30, and 45 meters per second. Air flows and air penetration around the Waid hydrofoil also occur in two ways. The first type of airflow around the hydrofoil is related to cavitation flows resulting from the angle of attack and the geometric shape of the foil. Most of these cavitation flows, which form at the tip of the hydrofoil, are accompanied by air penetration from the end of the foil that is second type of airflow.

As an example of the performed simulations, the results of the numerical simulation of the hydrofoil with the Waid section at the angle of attack of 7 degrees are shown in Figure 12. In this figure, the formation of cavitation bubbles around the hydrofoil can be seen well. After the partial formation of cavitation around the hydrofoil, the air flow will have the necessary space due to the pressure reduction around and at the end of the hydrofoil to penetrate these areas and help in the expansion of the formation of the cavitation bubble. In other words, the pressure drops around the hydrofoil due to cavitation makes it possible for the air flow to penetrate. Simultaneously, cavitation flow develops from the tip of the hydrofoil.

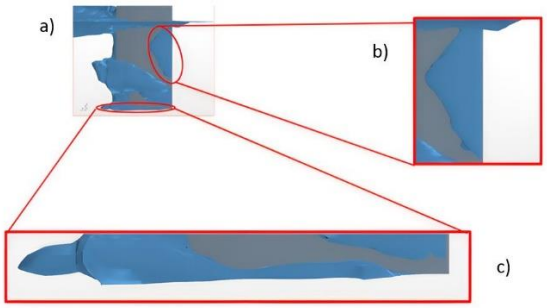

Fig. 12: Magnification of the supercavitation bubble around the Waid foil, (a) overall view, (b) cavitation bubble at the leading edge of the hydrofoil, (c) bubble formation due to the penetration of the bubble flow behind the hydrofoil

In Figure 13, the increasing trend of lift with an increase in the angle of attack can be seen. With an increase in the thickness of cavitation at higher angles of attack, as shown in Figure13, the lift coefficient is also observed to be at its lowest at a cavitation number of 0.9. In Figure14, the drag coefficient graph is displayed in different cavitation numbers. The maximum drag can be seen at the cavitation number of 0.9, and the reason for this is the absence of cavitation at this number. In this condition, there is the most contact between water and the hydrofoil surface. While with the reduction of the contact surface of the water and the hydrofoil, we generally see a decrease in this coefficient. As seen in Figure 15, the flow around the hydrofoil at an angle of 7 degrees is not completely dry and has a common boundary with water.

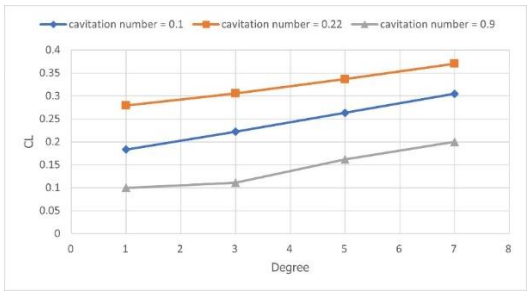

Fig. 13: Comparison of lift coefficients in different cavitation numbers for the Waid Foil

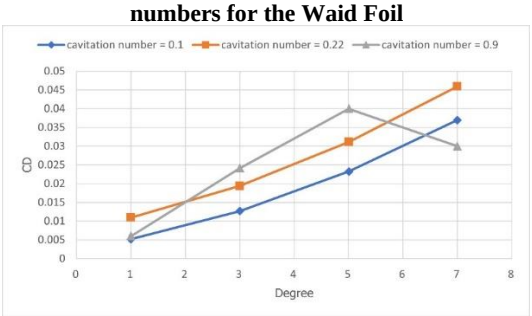

Fig. 14: Comparison of drag coefficients in different cavitation numbers for the Waid foil

This issue also happens at the angle of attack of one degree, so that the drag of the cavitation number is close to 0.9 or less than the drag of other cavitation numbers (Fig. 16). The reason for this can be due to the turbulence flows at the beginning and the tip of the foil. In other words, due to the arc and the shape of the foil geometry, at this angle, turbulence flows are created from the very beginning of the tip.

Figure 16(a) shows the fluid contours around the hydrofoil section from top view at an angle of 1 degree for a cavitation number of 0.22, and Figure 16(b) is specific to an angle of 3 degrees. The blue regions indicate the air or saturated vapor fluid around the foil, while the red regions represent water. With an increase in angle of attack, this stability in the drag coefficient may be attributed to the formation of bubbles around the hydrofoil.

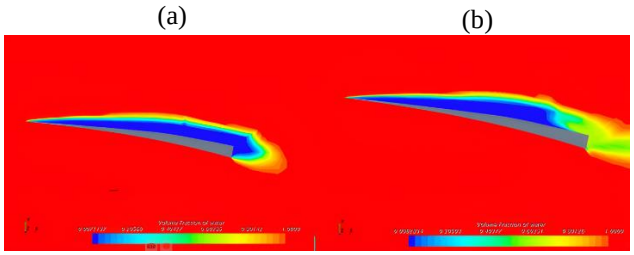

Fig. 15: The stream contour around the Waid section in cavitation number 0.22, (a) at an angle of 5 degrees, and (b) at an angle of 7 degrees.

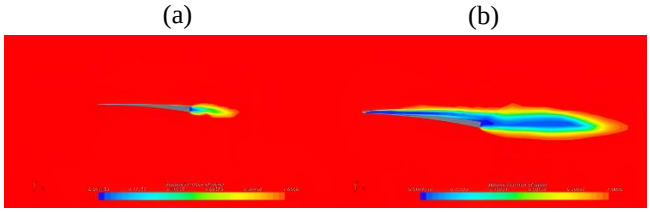

Fig. 16: The stream contour around the Waid section in cavitation number 0.22, (a) at an angle of 1 degree, and (b) at an angle of 3 degrees.

By reducing the cavitation number, the lift-to-drag ratio increases. This can be seen in Fig.17, and this ratio increase has a direct relationship with the dryness and complete dryness of the area, around the foil. The main reason for the reduction of the lift-to-drag ratio is related to the cavitation number. In other words, it depends on the dryness or wetness around the foil. The lift-to-drag ratio, up to an angle of 5°, is significantly higher at a cavitation number of 0.22 compared to the results at a cavitation number of 0.1. However, by entering a cavitation number of 0.9, the lift-to-drag ratio decreases due to the premature entry of the fluid flow around the hydrofoil into the fully wetted phase. The lift-to-drag ratio at a cavitation number of 0.22 at

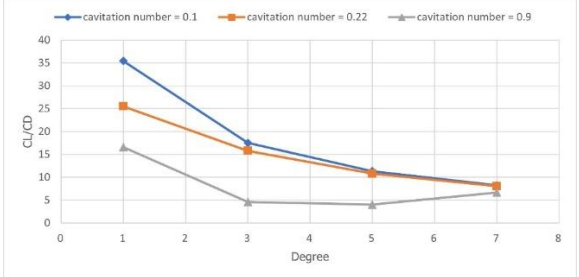

Fig. 17: Comparison of the ratio of lift coefficients to drag coefficients in different cavitation numbers for the Waid foil

an angle of 7 degrees is lower than the lift-to-drag ratio at a cavitation number of 0.1. The reason for this is simply the early entry of fluid flow. In other words, the factors affecting the hydrofoil efficiency include the angle of attack, which affects the turbulent flow behind the hydrofoil, and the cavitation number factor, which allows the formation of a dry area around the hydrofoil at lower numbers. This can also be understood from the pressure contours in Figure 18

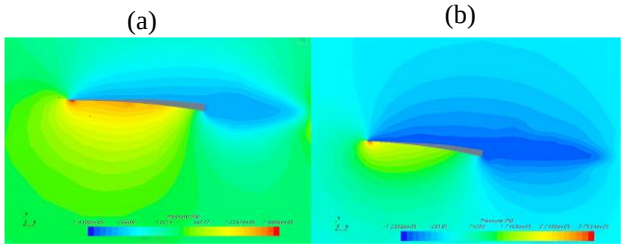

Fig. 18: The pressure contour around the Wiad section in cavitation number 0.22, (a) at an angle of 1 degree, and (b) at an angle of 3 degrees.

. Figure 19 also provides a good understanding of the effect of increasing the angle of attack on the hydrofoil. As the angle of attack increases, the dry surface of the hydrofoil increases too. As it can be seen from Figure 19, with an increase in angle of attack, the dry area of the hydrofoil decreases. This, in turn, reduces the hydrofoil's contact with water and affects the reduction in drag.

In Figure 19, images from top to bottom at angles of attack of 1, 3, 5, and 7 degrees are shown. From left to right in order is at a speed of 45, 30 and 15 meters per second, respectively. As seen in this figure, the wetness of the hydrofoil decreases with an increase in angle of attack.

Figure 20 compares pressure contours and fluid flow contours around the Waid hydrofoil, focusing on pressure concentration.

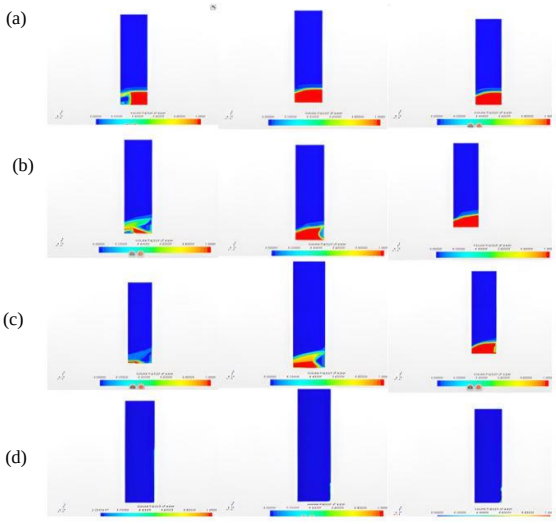

Fig. 19: Side view of the surface of the Waid-shaped hydrofoil and the wet and dry surface at four attack angles (a) 7 deg. (b) 5 deg. (c) 3 deg. and (d) 1 degree at a speed of 15, 30 and 45 m/s

In the cavitation profile of the hydrofoil, a low-pressure region is formed, and a comparison is also made with fluid flow contours. In this figure a comparison between the pressure contour and the cavitation flow around the hydrofoil at the cavitation number of 0.22 for the Waid section has been shown. It is clear in this figure that by reducing the pressure on the upper surface of the foil, we also see an increase in the amount of cavitation.

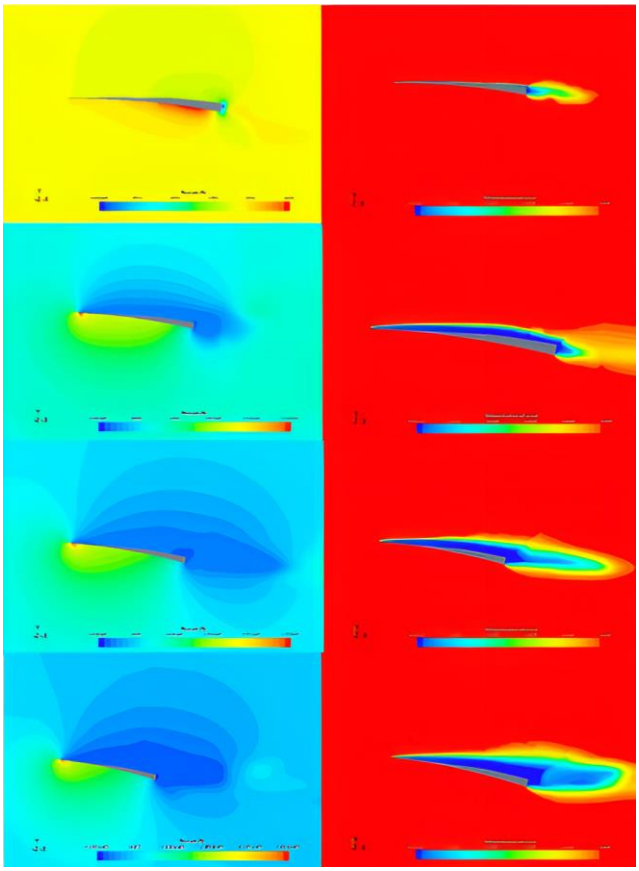

Fig. 20: Comparison of pressure and fluid flow streamlines around a hydrofoil Waid section at a cavitation number of 0.22

4. Conclusion

Among the methods of increasing the hydrodynamic lift force in high-speed craft is the use of hydrofoils. Some of these hydrofoils are surface piercing hydrofoils. According to the operational conditions, choosing the type of sections used in these hydrofoils is very important in their hydrodynamic behavior. In this article, instead of using conventional sections, supercavitating sections and specifically, the Waid section have been used in a surface piercing hydrofoil and numerically simulated. These sections can be modified to increase efficiency at various angles of attack for use in semi- submerged hydrofoils. In order to achieve an optimal semi-submerged hydrofoil, first the desired section (here the Waid section) is numerically simulated at different cavitation numbers and at different speeds and at different attack angles.

An increase in the angle of attack corresponds to an increase in lift and sometimes a decrease in the drag coefficient, but this does not mean an increase in efficiency.

In this simulation, the best angle of attack to achieve the optimal efficiency of the angle of attack of 1 degree has been identified. Also, considering that the target sections have different lift-to-drag ratios at different submersion depths, so it is recommended to use a combination of sections with different angles of attack for the design of a semi-submerged hydrofoil. In such a way that at any immersion depth of the hydrofoil, we can see a section with an optimal angle of attack (and with a high lift-to-drag ratio). According to the results obtained in this simulation, in the Waid section, by increasing the cavitation number, the ratio of lift to drag coefficient is about 10. This process continues until the section enter the completely wet phase. With this phase change, due to the increase of the wet surface of the foil, the ratio of lift to drag coefficients also decreases. Therefore, due to its high efficiency, the Waid cross-section is recommended for the design of semi-submerged hydrofoils.

5. References

[1] Waid, R.L., Lindberg, Z., Experimental and theoretical investigations of a supercavitating hydrofoil (1957)

[2] Afkar, H., Numerical simulation of flow with cavitation on ringed cavitator (2013)

[3] Tachmindji, A., Morgan, W., The design and estimated performance of a series of supercavitating propellers. In: Proc. of 2nd Office of Naval Research Symposium on Naval Hydrodynamics, pp. 489-532 (1958)

[4] Olofsson, N., Letter to the author and dr. s. a. kinnas (2001)

[5] Kermeen, R.W., Naca 4412 and walchner profile 7 hydrofoils in non-cavitating and cavitating flows. Rep. No 47, 1-21 (1956)

[6] Yao-tsu Wu, T., A free streamline theory for two-dimensional fully cavitated hydrofoils (1955)

[7] Furuya, Okitsugu. ''Nonlinear calculation of arbitrarily shaped supercavitating hydrofoils near a free surface." Journal of Fluid Mechanics 68, no. 1 (1975): 21-40.

[8] K. L. Wadlin, "Mechanics of ventilation inception," in Proceedings of the 2nd Symposium on Naval Hydrodynamics (Washington, DC, 1958), pp. 425–445.

[9] J. P. Breslin and R. Skalak, "Exploratory study of ventilated flows about yawed surface-piercing struts," NASA Technical Memorandum, Washington, DC, Technical Report No. 2-23-59W, 1959.

[10] K. I. Matveev, M. P. Wheeler, and T. Xing, "Numerical simulation of air ventilation and its suppression on inclined surface-piercing hydrofoils," Ocean Eng. 175, 251–261 (2019)

[11] S. Brizzolara and D. Villa, "Three phases RANSE calculations for surface-piercing supercavitating hydrofoils," in Proceedings of the 8th International Symposium on Cavitation (Singapore, 2012).

[12] C. Xu, J. Huang, Y. W. Wang, X. C. Wu, C. G. Huang, and X. Q. Wu, "Supercavitating flow around high-speed underwater projectile near free surface induced by air entrainment," AIP Adv. 8, 035016 (2018).

[13] S. T. Chen, W. W. Zhao, and D. C. Wan, "CFD study of free surface effect on flow around a surface-piercing cylinder," in Proceedings of the 14th ISOPE Pacific-Asia Offshore Mechanics Symposium (Dalian, China, 2020).

[14] R. L. Waid, Z. Lindberg, Experimental and theoretical investigations of a Supercavitating hydrofoil (1957).

[15] R. W. Kermeen, Experimental investigations of three-dimensional effects on cavitating hydrofoils (1960).

[16] B. R. Parkin, Experiments on circular arc and flat plate hydrofoils in Non-cavitating and full cavity flows (1956).

[17] V. E. Johnson, Theoretical determination of low-drag supercavitating hydrofoils and their two-dimensional characteristics at zero cavitation number, National Advisory Committee for Aeronautics, 1957.

[18] M. P. Tulin, Supercavitating flows - small perturbation theory, Journal of Ship Research 7 (1964) 16–37.

[19] N. E. Fine, S. Kinnas, A boundary element method for the analysis of the flow around 3-d cavitating hydrofoils, Journal of ship research 37 (1993) 213–224.

[20] S. Mishima, S. A. Kinnas, A numerical optimization technique applied to the design of two-dimensional cavitating hydrofoil sections, Journal of ship research 40 (1996) 28–38.

[21] Y. Young, S. Kinnas, Analysis of supercavitating and surface-piercing propeller flows via bem, Computational Mechanics 32 (2003) 269–280.

[22] J. Royset, L. Bonfiglio, G. Vernengo, S. Brizzolara, Risk-adaptive set based design and applications to shaping a hydrofoil, Journal of Mechanical Design 139 (2017) 101403

[23] Brizzolara, Stefano," A new family of dual-mode supercavitating hydrofoils." Fourth International Symposium on Marine Propulsors. 2015.

[24] G. Vernengo, L. Bonfiglio, S. Gaggero, S. Brizzolara, Physics-based design by optimization of unconventional supercavitating hydrofoils, Journal of Ship Research 60 (2016) 187–202.

[25] Y. Wang; C. Huang; T. Du; R. Huang, Y. Zhi; Y. Wang, Z. Xiao, Z. Bian, "Research on ventilation and supercavitation mechanism of high-speed surface-piercing hydrofoil", Physics of Fluids, 34, 023316 (2022)

[26] Ferziger, J.H., Peric, M., Computational methods for fluid dynamics. 3rd rev. ed., Springer-Verlag, Berlin (2002)
[27] Koop, A.H., Hoeijmakers, H., Numerical simulatin of unsteady three-dimensional sheet cavitation. University of Twente Enschede, The Netherlands (2008)
[28] Harwood, C., The hydrodynamic and hydro-elastic responses of rigid and flexible surface piercing hydrofoils in multi-phase flows. Ph.D. thesis (2016)
[29] Young, Y.L.J., Numerical modeling of supercavitating and surface-piercing propellers. The University of Texas at Austin (2002)